RL-TR-94-108
Final Technical Report
August 1994

AD-A285 672

PICOSECOND OPTOELECTRONIC AND-GATE

Picotronix, Inc.

Steven L. Williamson

APPROVED FOR PUBLIC RELEASE; DISTRIBUTION UNLIMITED.

Rome Laboratory
Air Force Materiel Command
Griffiss Air Force Base, New York

This report has been reviewed by the Rome Laboratory Public Affairs Office (PA) and is releasable to the National Technical Information Service (NTIS). At NTIS it will be releasable to the general public, including foreign nations.

RL-TR-94-108 has been reviewed and is approved for publication.

APPROVED: Reinhard K. Erdmann

REINHARD K. ERDMANN
Project Engineer

FOR THE COMMANDER: Luke L. Lucas

LUKE L. LUCAS, Colonel, USAF
Deputy Director
Surveillance & Photonics

If your address has changed or if you wish to be removed from the Rome Laboratory mailing list, or if the addressee is no longer employed by your organization, please notify RL (OCPA) Griffiss AFB NY 13441. This will assist us in maintaining a current mailing list.

Do not return copies of this report unless contractual obligations or notices on a specific document require that it be returned.

REPORT DOCUMENTATION PAGE

Form Approved
OMB No. 0704-0188

1. AGENCY USE ONLY (Leave Blank)	2. REPORT DATE	3. REPORT TYPE AND DATES COVERED
	August 1994	Final Mar 93 - Aug 93

4. TITLE AND SUBTITLE
PICOSECOND OPTOELECTRONIC AND-GATE

5. FUNDING NUMBERS
C - F30602-93-C-0067
PE - 62702F
PR - 4600
TA - P1
WU - PQ

6. AUTHOR(S)
Steven L. Williamson

7. PERFORMING ORGANIZATION NAME(S) AND ADDRESS(ES)
Picotronix, Inc.
P O Box 130243
Ann Arbor MI 48113-0243

8. PERFORMING ORGANIZATION REPORT NUMBER
N/A

9. SPONSORING/MONITORING AGENCY NAME(S) AND ADDRESS(ES)
Rome Laboratory (OCPA)
25 Electronic Pky
Griffiss AFB NY 13441-4515

10. SPONSORING/MONITORING AGENCY REPORT NUMBER
RL-TR-94-108

11. SUPPLEMENTARY NOTES
Rome Laboratory Project Engineer: Reinhard K. Erdmann/OCPA/(315) 330-4455

12a. DISTRIBUTION/AVAILABILITY STATEMENT
Approved for public release; distribution unlimited.

12b. DISTRIBUTION CODE

13. ABSTRACT (Maximum 200 words)

Logic gates based on conventional high speed detectors are limited by the recovery time, which can be over a hundred pico seconds. High speed direct detection with picosecond response near 0.85 um has been successfully demonstrated in LT grown GaAs structures using interdigitated electrodes. These can form the key element in an optical AND GATE used for demultiplexing digital data at rates of up to 100 G bits. In this project, new materials based on LT grown InGaAs are developed and tested for their suitability at the 1.3 and 1.5 um wavelengths, where single mode fiber capable of supporting such rates operates. The results to date extend pico second range responses to around 1.06 um, but basic physical properties still preclude full extension to the desired wavelengths allowed by the range of transparency. Successful applications have resulted at the shorter wavelengths, and the results of these studies will facilitate the on-going material development needed to further extend the range of this new device technology.

14. SUBJECT TERMS	15. NUMBER OF PAGES
Optical gate, AND gate, Fiber Optic Switch, High speed detector, Low temperature grown InGaAs	36
	16. PRICE CODE

17. SECURITY CLASSIFICATION OF REPORT	18. SECURITY CLASSIFICATION OF THIS PAGE	19. SECURITY CLASSIFICATION OF ABSTRACT	20. LIMITATION OF ABSTRACT
UNCLASSIFIED	UNCLASSIFIED	UNCLASSIFIED	UL

NSN 7540-01-280-5500

Standard Form 298 (Rev. 2-89)
Prescribed by ANSI Std. Z39-18
298-102

Summary of Completed Project

The goal of this program was the demonstration of the key components that would set the stage for the development of a picosecond optoelectronic AND-gate. The AND-gate would have a temporal resolution < 10 ps (10^{-11} s). At the heart of the AND-gate is a new optoelectronic picosecond autocorrelator, known as a Sampling Optical Temporal Analyzer, or SOTA. The SOTA is a device comprised of a picosecond photodetector integrated to an equally fast photogate. The device is capable of detecting and sampling optical pulses of single-picosecond duration. The output is a quasi-dc electrical signal that has an amplitude representative of the correlation between the optical pulses incident on the detector and gate. Only when the two optical pulses are both present and synchronized will current flow through the SOTA. The SOTA is completely solid-state and operates jitter-free.

As part of this program we began development of InGaAs photoconductors with picosecond carrier lifetimes. Initially, we worked on $In_{0.25}Ga_{0.75}As$ for operation out to 1100 nm. In addition to fast carrier lifetime, these new materials must exhibit low dark current and high mobility. We will see later that achieving all three ingredients is difficult but not impossible.

The specifications set forth for the SOTA-based AND-gate are as follows:

- Wavelength range..... 350-1300 nm
- Contrast ratio..... < 100:1
- Temporal response ..... < 7ps

We have fabricated and tested this device to determine its ultimate speed, sensitivity, and dynamic range. The SOTA's system response was found to be 1.4 ps with a sensitivity of 100 pW (noise equivalent power). This is now the world's fastest, most compact, ultrasensitive, picosecond optical waveform analyzer. It is completely solid-state, operates free of jitter and has a measured dynamic range of 80 dB.

TABLE OF CONTENTS

LIST OF ILLUSTRATIONS

1. INTRODUCTION

In 1991, Williamson and coworkers reported on a picosecond-resolution, high-sensitivity photodetector based on low-temperature grown GaAs (LT-GaAs).[1] LT-GaAs is the name given to GaAs grown at low temperature using molecular beam epitaxy (MBE). GaAs grown between 200°- 400°C is nonstoichiometric in its structure. Upon post annealing at 600° C, excess arsenic within the GaAs coalesces into precipitates uniformly distributed throughout the bulk GaAs epilayer. These precipitates serve to trap photogenerated carriers within as little time as 1 ps from the moment they are generated. This trapping process arrests the flow of current in the photoconductor, giving LT-GaAs photoconductors their ultrafast response time.

For a photodiode, when the spacing between the contacts forming the detector is reduced, the speed of the detector increases with little change in sensitivity. In a photoconductive-type detector, by contrast, a reduction in spacing increases the *sensitivity* with little change occurring to the speed. By reducing this spacing, we decrease the carrier transit time across the semiconductor gap to a value comparable to the carrier lifetime and thereby increase the photocurrent gain to a value approaching unity.[2] For a carrier lifetime of 1 ps, this condition is met when the electrode spacing, i.e., the actual gap between electrodes, is 0.1 μm. With unity gain, the responsivity of a LT-GaAs photoconductive detector becomes comparable to that of a photodiode, while its speed is still dominated by its (sub)picosecond intrinsic carrier lifetime. Fig. 1 is an SEM photograph taken of this type photodetector. The multi-hundred gigahertz bandwidth of the photogenerated signal requires that the detector be located between coplanar electrodes to assure good coupling to the propagating mode and to minimized parasitic effects.

Fig. 2 shows a family of traces taken using this photodetector for different input pulse energies. The measurements were made using the technique of electro-optic sampling.[3] At low light, the response is 1.2 ps, corresponding to a 3-dB bandwidth of 375 GHz. The four signals have peak amplitudes of 6, 3.5, 0.6, and 0.06 V generated using 22, 8.3, 0.83, and 0.04 pJ, respectively. We see that a 500-fold increase in intensity expands the response only slightly from 1.2 to 1.5 ps. Under similar experimental conditions, a high-speed photodiode would suffer significant temporal broadening from space charge and low-frequency gain by photo-induced band bending.[4] Thus, the LT-GaAs photoconductive detector avoids the usual restriction of photodiodes to pulse energies below 0.1 pJ to achieve optimum bandwidth performance. A pulse energy of 22 pJ produces a signal of 6 V. This corresponds to an on-state resistance of 30 Ω.

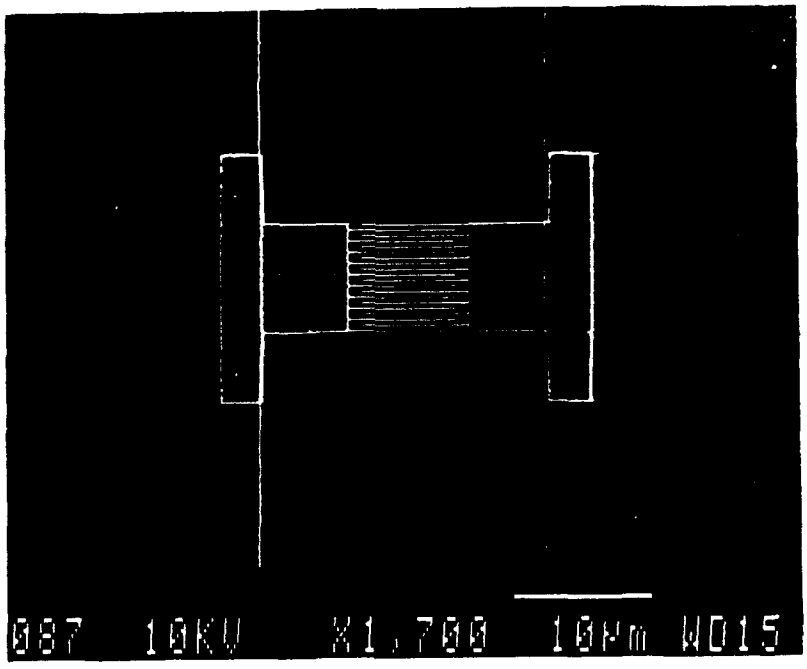

Fig. 1 375-GHz photodetector based on low-temperature-grown GaAs (LT-GaAs). The material has a subpicosecond intrinsic response time. An electron mobility > 100 cm^2/V-S and 0.2-µm interdigitated electrodes combine to push the sensitivity of the detector to 0.1 A/W, comparable with conventional photodiodes. The detector is shown bridging 20-µm electrodes that form a coplanar stripline. The area of the detector is 6x7 μm^2. A bias voltage of 8 V can be applied without breakdown.

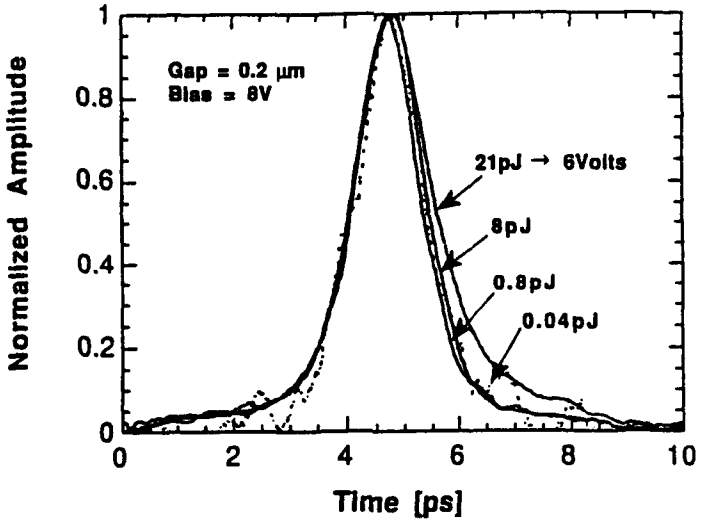

Fig. 2 Set of four signals generated from the LT-GaAs photodetector. The fastest response is 1.2 ps (full-width-at-half-maximum), with a measured 3-dB bandwidth of 375 GHz. Peak amplitudes of 6, 3.5, 0.6, and 0.06 V are generated using 22, 8.3, 0.83, and 0.04 pJ/pulse, respectively. A signal of 6 V corresponds to an on-state resistance of 30 Ω. The off-state resistance is 10 MΩ.

This high efficiency switching, combined with the single-picosecond response time, uniquely qualifies the LT-GaAs photoconductive detector for dual operation as either an ultrafast high-sensitivity detector or ultrafast high-efficiency gate.

We took advantage of the dual functionality of the detector to construct a simple picosecond autocorrelator using two photoconductive-type detectors. This device is depicted in Fig 3. It is functionally the same as a picosecond optoelectronic AND-gate. Current only flows through the device when both detectors are simultaneously activated. The semiconductor autocorrelator is not new, although it has been limited to applications using high peak power optical pulses.[5,6] By using LT-GaAs photodetectors, this technique becomes a powerful tool for detecting and analyzing ultrafast, ultraweak optical signals. We call this modified autocorrelator the Sampling Optical Temporal Analyzer - SOTA.

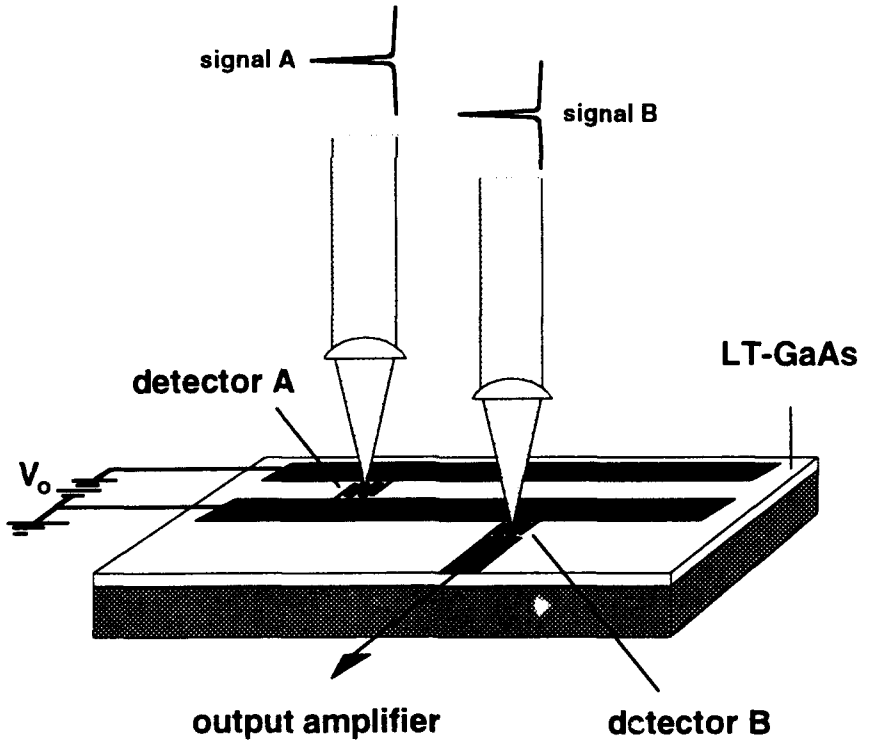

Fig. 3 Schematic diagram of the picosecond optoelectronic autocorrelator. Signals A and B must arrive simultaneous (accounting for propagation delay on the transmission line) before current pass through to the amplifier.

The peak output current from detector B is determined from the expression,

$$I_B = a^2 b^2 P_A P_B V_A Z$$

where, $a=qn/hv$ and $b=\mu_n t_t/L^2$

with, q is the electronic charge
n is the detector quantum efficiency (includes all reflections)
hv is the photon energy
μ_n is the electron mobility (holes play a less-important role)
t_t is the intrinsic carrier lifetime of the semiconductor
L is the electrode gap dimension forming the detector
P_A is the incident optical power (peak) on detector A
P_B is the incident optical power (peak) on detector B
V_A is the bias voltage on detector A
Z is the characteristic load impedance of the SOTA

For a detector quantum efficiency, n=0.10, $hv=1.5\times10^{-19}$ J (λ=1300 nm), $\mu_n=100$ $cm^2/_{V\text{-}S}$, $t_t=5\times10^{-12}$s, and L=1 μm, $P_A=P_B=4$ W, $V_A=10$ volts, and Z=50 Ω, we have I_B = 20 mA, corresponding to 0.1 pC per 5-ps optical pulse.

2. QUESTIONS TO BE ANSWERED DURING THIS PROGRAM

The main objective of this project was to demonstrate the feasibility of integrating a picosecond optical detector with a picosecond laser activated sampling gate. Questions to be answered during this program were:

- What is the ultimate speed for the SOTA and what is the limiting factor?
- What sensitivity and dynamic range can be achieved?
- What is the relationship between speed and sensitivity?
- Can LT-InGaAs replace LT-GaAs for long wavelength applications?

3. DESCRIPTION OF WORK CARRIED OUT

To accomplish these goals, we needed to grow LT-GaAs epilayers, design an appropriate electrode geometry to assure high speed, characterize the SOTA, and investigate the feasibility of using indium-based III-V compounds. We describe each of these areas and offer suggestions for future improvements.

LT-GaAs material

The semiconductor material required for achieving the fast carrier lifetime is grown using unconventional MBE techniques. Unlike traditional MBE, where the substrate temperature is kept between 600° C and 850° C, the growth temperature for our application is considerably lower and more stringent. We need to grow the epilayer at or just a few degrees above the critical temperature for formation of a single-crystal epitaxial layer, that is 190° C to 210°C.

GaAs grown in this temperature range exhibits unusual properties resulting from excess arsenic (~1%).[7] The arsenic is incorporated mainly in interstitials of the crystal, which coalesce into micro-precipitates with a subsequent short-duration high-temperature (600°C) anneal. The most important feature exhibited by LT-GaAs is its ultrafast photocarrier lifetime. As we approach the temperature at which polycrystalline GaAs forms the As concentration increases and the carrier lifetime becomes shorter.

Subpicosecond measurements are made using an all-optical pump-probe technique that measures the change in reflectivity at the surface of a semiconductor.[8] For this experiment, two 0.1 ps laser beams are positioned concentrically on the surface of the LT-GaAs epilayer. The larger diameter beam (pump) photogenerates the carriers while the smaller beam (probe) senses the slight difference in reflectivity that results from the plasma-induced change in dielectric constant. The probe pulse is continuously delayed in time to map out the time evolution of carrier generation and recombination/trapping that comprise the material's intrinsic response. Fig. 4 shows the lifetime of the fastest LT-GaAs material used for this program. The carrier lifetime is almost as fast as the 0.1 ps duration pump/probe pulses. The epilayer was grown to a thickness of 1.5 μm at a temperature of 190° C on a (100)-oriented GaAs substrate with a Ga/As flux ratio of 20. After the epitaxial layer was grown it was anneal at 600° C for 10 min. in an As overpressure.

In addition to subpicosecond carrier lifetime, LT-GaAs is also highly resistive ($\geq 10^7$ Ω-cm) and maintains perfect crystallinity as measured using high-resolution TEM and X-ray diffraction. The electron mobility can be as high as 150 cm^2/V-s and the dielectric breakdown can exceed 500 kV/cm. The combination of ultrafast carrier lifetime, high mobility, and high resistivity provide the key ingredients for development of ultrafast, high-sensitivity photodetectors. Despite the virtues of LT-GaAs, much research is still required to assure quality control. The optimal growth process is not yet known and inconsistencies in temperature calibration between different foundries (and even different machines) exist.

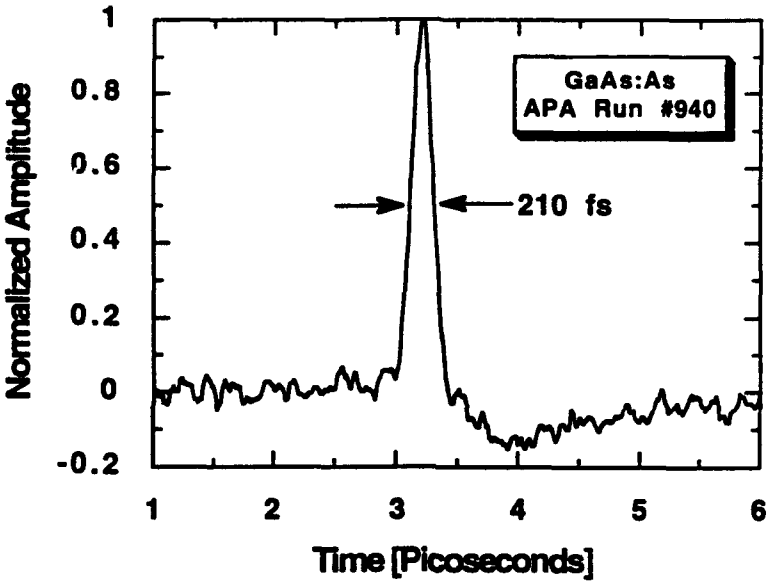

Fig. 4 All-optical time-resolved reflectivity measurement taken of the surface of a LT-GaAs epilayer. The 1.5-μm thickness epilayer was grown at 200° C and post annealed at 600° C for 10 min. in an As overpressure. Accurate measurement of the photogenerated carrier density can be made without the need for electrical contacts.

For example, Fig. 5 shows the results of another LT-GaAs sample grown presumably under identical conditions by another foundry. The carrier lifetime is 3 ps, over 10 times that found for the previous sample. The problem stems from the need to extrapolate calorimeter data from 500° C down to 200° C. We also must make the assumption that the top surface of the substrate is at the same temperature as the surface contacting the calorimeter. These issues become critical when tolerances of only a few degrees in substrate temperature amount to dramatic changes in material properties.

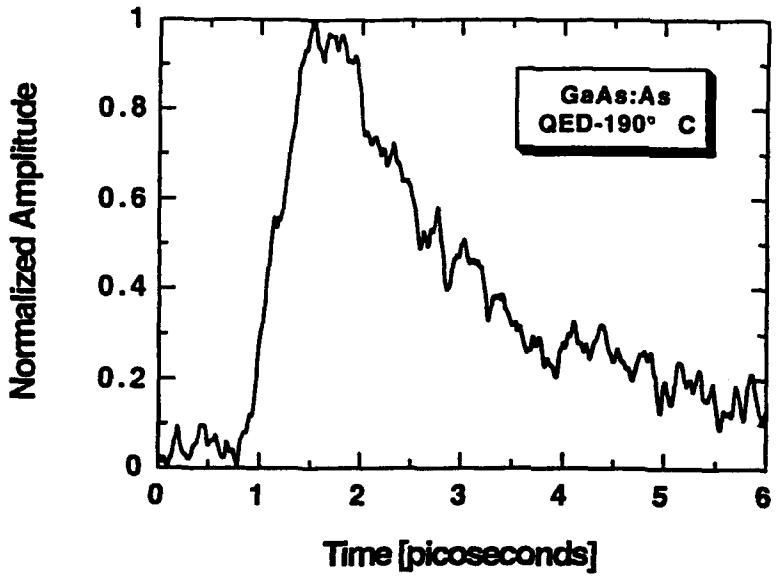

Fig. 5 Reflectivity measurement taken of another LT-GaAs grown at a different facility, presumably under the same conditions as the sample used for Fig. 4.

Detector design

To take full advantage of the unique properties of LT-GaAs we need to design the electrode geometry to attain high sensitivity. As previously mentioned, a detector based on LT-GaAs is akin to a photoconductor rather than a photodiode. Sensitivity for a photoconductor is related to the so-called photocurrent gain, $G=\tau/t_r=\mu_n E/L$. Where, τ is the carrier lifetime, t_r is the carrier transit time, μ_n is the electron mobility, E is the electric field, and L is the electrode spacing. Decreasing the carrier transit time across the semiconductor gap to a value comparable to the carrier lifetime increases the photocurrent gain to a value of unity.

We achieve this performance by using a simple metal-semiconductor-metal (MSM) interdigitated electrode structure with finger spacing and width adjustable down to 0.2 μm. MSM structures could, in principle, be designed for a photocurrent gain greater than unity, making for a detector that exceeds the sensitivity of a photodiode. The need for low-barrier ohmic contacts to permit the injection of new carriers and electrode spacings below 0.1 μm prevent the incremental improvement from being cost effective.

Improvement in sensitivity as functions of electrode spacing and applied bias have been measured. We have fabricated and tested four interdigitated MSM photoconductive detectors of various finger width/spacing. The detectors were fabricated of 300Å/200Å Ti/Au using a JEOL JBX 5DIIF direct-write electron beam lithography system. Each detector has an active area of 50x50 μm^2 and a finger width/spacing of either 2.0 μm, 1.0 μm, 0.5 μm, or 0.2 μm.

The I-V curves were measured and plotted in Fig. 6. The values found for the 0.5 μm, 1.0 μm, and 2.0 μm are comparable to dark current densities (current/active area) found with state-of-the-art *p-i-n* photodiodes. The 0.2 μm detector shows considerably higher dark current. For constant electric field, we find the current density for the 0.2 μm detector is, in fact, comparable to the other three. A bias of 8 volts applied to the 0.5-μm detector corresponds to an electric field of 160 kV/cm and produces a dark current density of 32 $pA/\mu m^2$. An electric field of 160 kV/cm across the 0.2-μm detector is obtained with a bias of 3.2 volts, corresponding to a dark current density of 45 $pA/\mu m^2$.

The photocurrent for the four detectors was measured as functions of applied bias and the finger width/spacing. As expected, there is little change in the photocurrent generated as the laser spot size is reduced from 50 μm down to 10 μm. If the applied electric field and the total number of photocarriers is kept constant, the photocurrent generated will also remain constant, independent of the laser spot size. For these experiments we used a HeNe laser focused to 25 μm diameter. Fig. 7 shows the results for two incident power levels. We see that the photocurrent scales nearly linearly with increased bias. We also note a linear increase in photocurrent with decreasing electrode spacing and increasing optical power. With a bias of 6 volts the 0.2 μm detector has a responsivity of 0.1 A/W. These measurements have been made without using AR coatings on the detector or accounting for losses due to metalization (which is avoidable *via* backside illumination). We believe a responsivity exceeding 0.5 A/W is attainable for practical picosecond detectors.

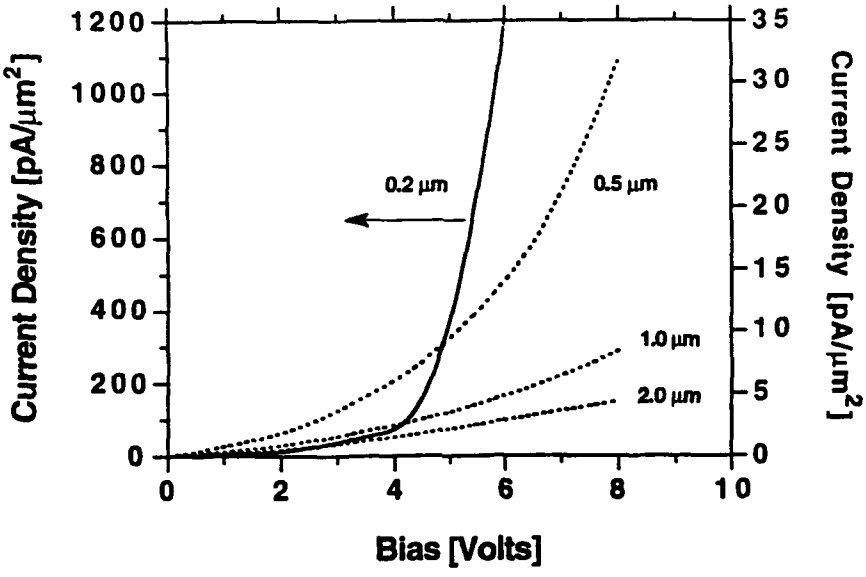

Fig. 6 I-V curves for the four MSM detectors. The dark current density for the 0.2 μm detector is plotted using the left-side ordinate. The remaining three detectors are plotted using the right-side ordinate.

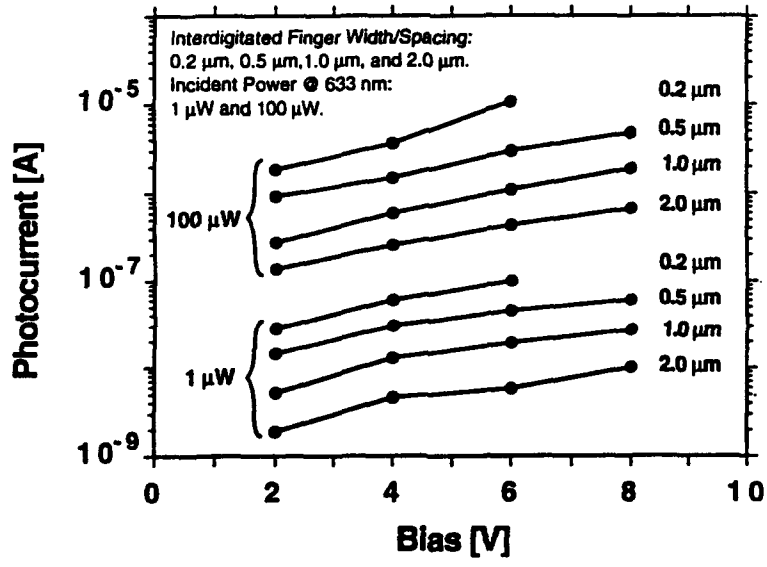

Fig. 7 Photocurrent for the four MSM detectors as a function of the applied bias. The four detectors are plotted at two optical power levels. The 0.2 μm detector biased to 6-V shows a responsivity of 0.1 A/W.

Fig. 8 summarizes the results for the 0.2-μm detector. Plotted are the photogenerated electrical pulse amplitude and the corresponding on-state conductance of the detector as functions of the pulse energy. For optical pulse energies of 20 pJ the resistance of the detector drops from >10 MΩ down to 30 Ω in 1 ps. This suggest that one photoconductive detector can function either as a picosecond detector or a picosecond gate, according to the incident pulse energy. This dual-function photoelement gives the SOTA its unprecedented performance.

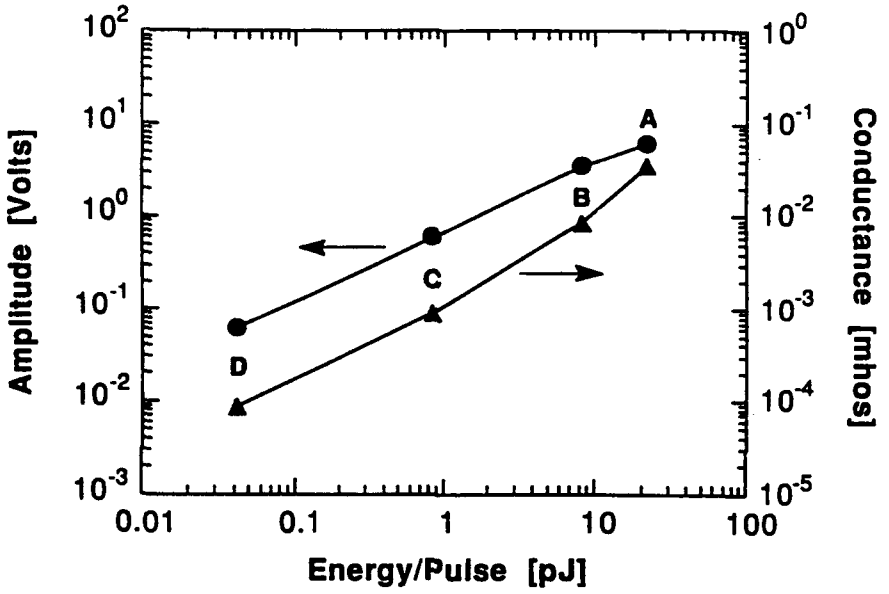

Fig. 8 Peak amplitude and conductance of the signals shown in Fig. 2 plotted against the incident pulse energy. This plot highlites the dual functionality essential for the SOTA.

SOTA design

The best performance to date for the SOTA incorporates the same coplanar transmission line structure shown in Fig. 1. This configuration integrates the interdigitated MSM photodetector into the coplanar transmission line and assures good coupling of the electrical signal to the propagating mode and also eliminates the possibility of parasitic losses from wire bonds and bonding pads. A voltage is applied across the two electrodes and adjacent fingers of the detector. Two SOTA designs were fabricated with the finger width/spacing of 0.2 μm or 1.0 μm, with the

detector and gate areas fixed at $10 \times 10\ \mu m^2$. An optical signal on the detector initiates a current transient that generates an electrical replica. The electrical signal propagates in both directions away from the detector along the transmission line.

Fig. 9 graphically depicts the experimental layout for the SOTA. The sampling gate is positioned 200 μm from the detector, or approximately 2 ps in propagation time, and connected to the ground electrode of the transmission line. The distance between the detector and gate is kept short to reduce dispersion. The gate electrode is normal to the transmission lines for a distance of 3 mm to avoid any rf coupling. When the gate is activated its resistance drops below 100 Ω and current from the ground electrode transfers across the gate. The sampled signal is effectively mixed down to quasi-DC frequencies and can than be measured using conventional electronics. In fact, a portable digital voltmeter can measure the signal directly. To map out the entire electrical signal (*ie.* optical replica), we introduce a delay between the the gate pulse and optical signal to sample each slice of time. Recently, we have shown that rapid scanning of the relative delay is also possible and offers the user the ability to "see" the optical event in real time.

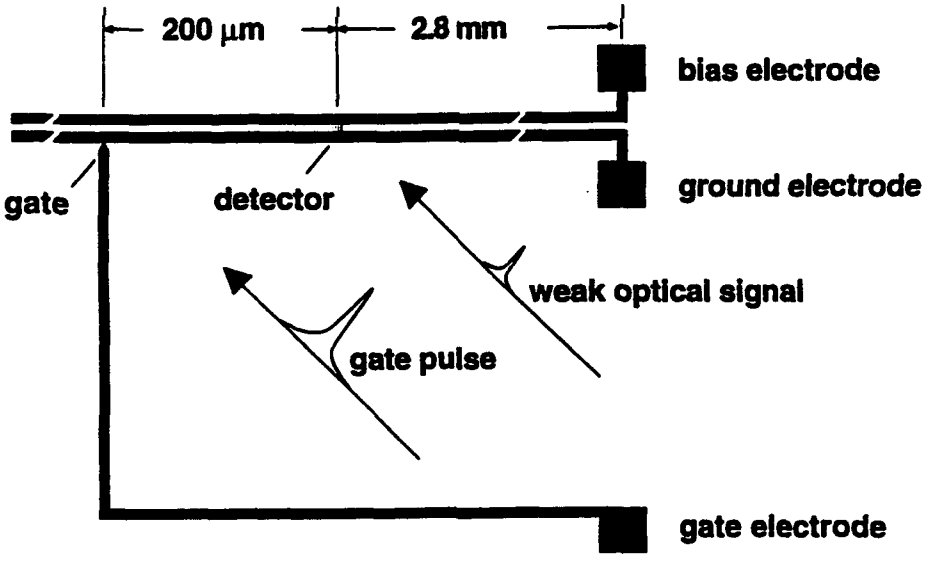

Fig. 9 Fabrication layout for the SOTA. The 200 μm distance between the detector and gate amounts to a propagation time of 2 ps. The first reflection that returns from the end of the transmission line takes 60 ps to arrive at the gate.

Fig. 10 is a photomicrograph of the actual SOTA device. The matrix in the middle of the pattern is a set of two rows of photodetectors used for the sensitivity measurements discussed earlier. (We omitted the fifth detector, with finger width/spacing of 0.1 μm, from our results due to inconsistencies in the data). From this photomicrograph we gain an appreciation for the size of the 10x10 μm^2 detector and gate. These dimensions are required to hold the rc time constant to less than 1 ps. A 0.2 μm detector of this size has a capacitance of 4 fF. When integrated into a 90 Ω impedance transmission line the theoretical response is 0.35 ps.

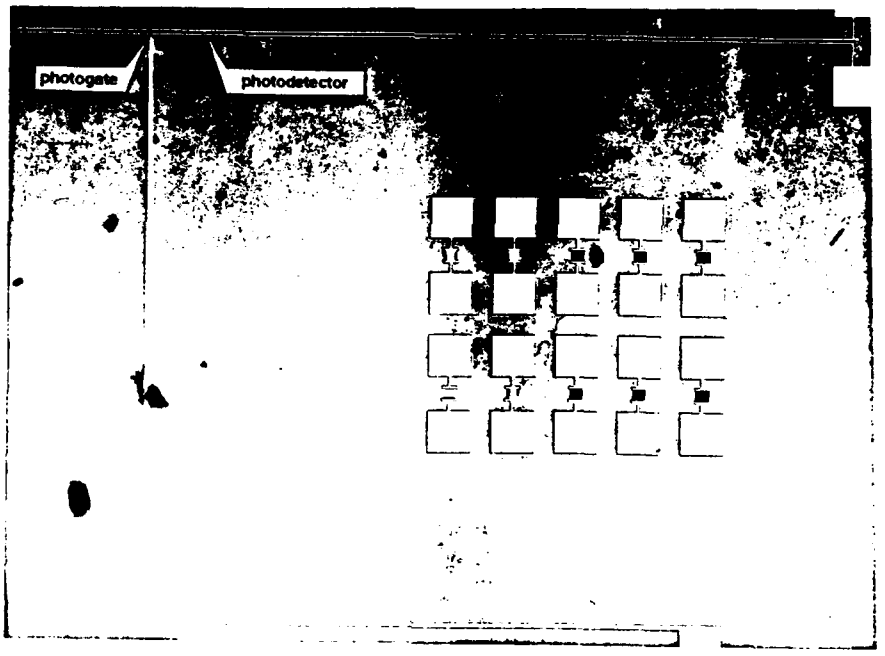

Fig. 10 Photomicrograph of the actual SOTA layout. The matrix of patterns in the center are the detectors used earlier for measuring the responsivity (shown in Figs. 6 and 7).

Instead of wire bonding individual SOTAs for testing, we opted for leaving the SOTAs on the wafer and making electrical contact using mechanical probes. Fig. 11 is a photograph of the actual experimental apparatus. The mechanical probes and the stage holding the wafer are designed to move independent of one another. This setup greatly speeds the testing process and enables quick isolation to prevent electro-static discharge. The signal gated to the gate electrode is sent to high gain current preamplifier and lock-in amplifier. The lock-in is tuned to a specific frequency, which is also the frequency at which the optical signal under study is being modulated. Amplitude modulation of this signal is accomplished using a mechanical chopper placed in the beam. The lock-in amplifier filters all signals except those having the precise frequency and phase of the mechanical chopper.

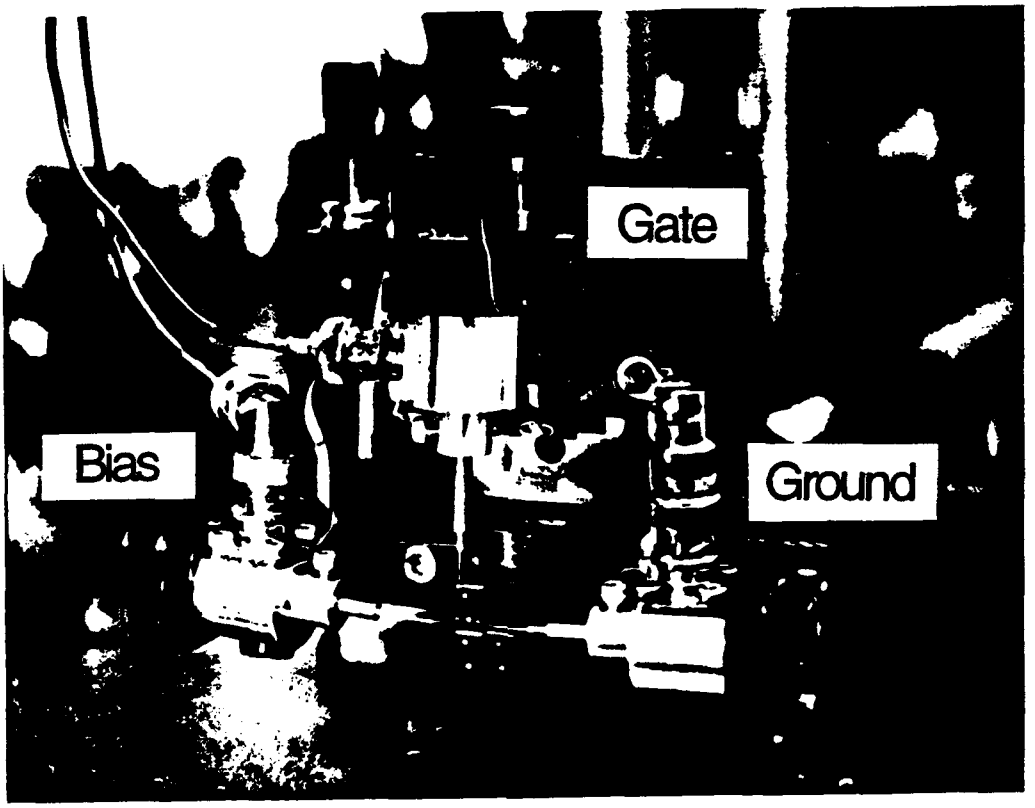

Fig. 11 Experimental apparatus for testing the SOTA. The bias, gate, and ground probes make contact to their respective bond pads.

4. RESULTS

Temporal response of LT-GaAs-based SOTA

Fig. 12 shows the system response for the SOTA. The measurement was made with the optical signals incident on the detector and gate both being of 0.1 ps duration. The response of the SOTA is 1.4 ps. This the fastest, high sensitivity detector/analyzer yet demonstrated. The deconvoluted speed of either the detector or gate is 1.0 ps.

We see that the response is not symmetric, indicating the SOTA is in fact not behaving like an ideal autocorrelator. The tail shown on the trailing side of the pulse persists for 30 ps. The tail results from a combination of capacitive and inductive reactance that couples charge through the

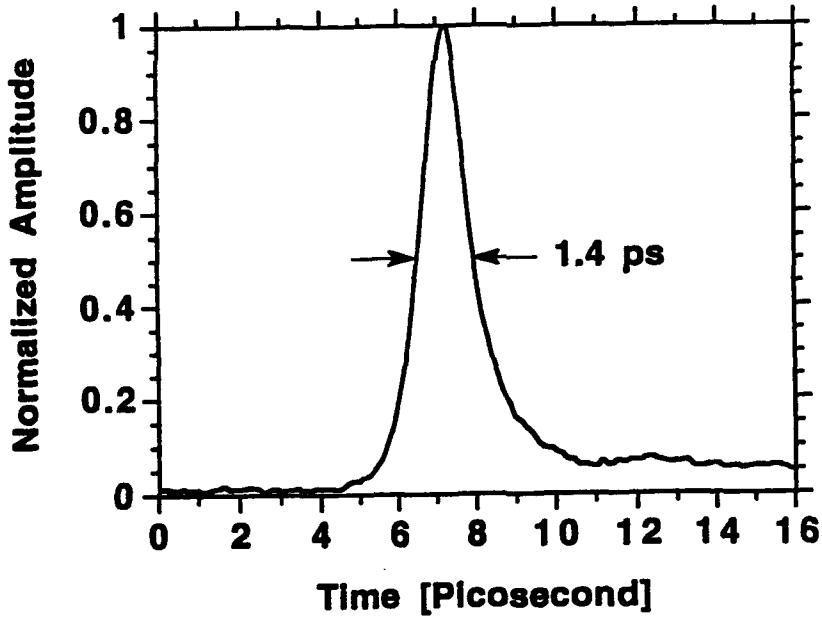

Fig. 12 Temporal response of the SOTA.

interdigitated sampling gate and onto the gate electrode. The net charge is zero and is transferred without the need of the optical gate pulse. When the optical pulse does arrive, say 10 ps after the electrical pulse has past, the gate electrode is still residually charged with a rapidly decaying bipolar pulse. The gate electrode is not of constant impedance and effectively reflects the coupled signal, in a backward-propagating mode, onto the gate.

Activating the gate then transfers charge *off the gate electrode* and onto the ground electrode, appearing as though charge is being transferred onto the gate electrode. Our lock-in amplifier cannot tell which direction charge is transferred. It only filters and amplifies signals that are produced by the *combined* action of detection and gating, via the technique of difference-frequency mixing. Charge that is reactively-coupled onto the gate electrode will not necessarily be amplified by the lock-in. Only coupled charge that is subsequently gated back to the transmission line, due to the presence of the optical gate pulse, will be properly filtered and amplified by the lock-in. After 30 ps this displacement current pulse decays away, with no net effect on the balance of charge. Only through the process of mixing at our photogate is the signal revealed. The tail can be greatly reduced by using a straight gap (not interdigitated) for the sampling gate to reduce the reactance. The gate pulse is always coherent and thus can be focused to 1 μm or less, therefore allowing small gaps to be used.

The fact that the leading edge of the response is flat and holds to the baseline indicates that the LT-GaAs indeed has an extremely fast carrier lifetime with no residual tail.

Sensitivity of the SOTA

We have pushed the sensitivity of the SOTA to 100 pW (NEP). The gate pulse energy for this result was 10 pJ. The useful dynamic range now extends from an average power of 100 pW to 10 mW, or 80 dB. A dynamic range of 80 dB surpasses by a factor of a 1000 the state-of-the-art in streak camera technology. Although the sensitivity is now comparable to the streak camera, it still remains 2 orders of magnitude away from the Johnson noise limit of 1 pW. We are now limited by laser noise fluctuations. Instabilities in the amplitude and beam position are responsible for the existing noise. Our colliding pulse mode-locked laser has 10% amplitude ripple and is prone to slight beam movement, caused by the use of two intercavity dye jets. The problem actually stems from the Schottky barriers that form the MSM contacts of the gate. The barrier at

the junction has an internal electric field that permanently biases the gate to a few hundred millivolts. The intense gate pulse can generate an electrical signal as large as 100 mV in amplitude.

What makes the interdigitated gates unique is the alternating polarity of the electric field between adjacent fingers. Photovoltaic current generates opposing electrical signals that effectively cancel one another. However, when the electrical signal being sampled is as weak as 1 pA. residual current generated at the gate does become significant. Discrimination *via* the lock-in by tuning away from the modulated (chopping) frequency of gate signal and to the sum frequency of the gate + detector signal can eliminate a great deal of this background signal. Unfortunately, if the gate signal fluctuates too much, the signal is no longer of narrow bandwidth centered at the modulated frequency and can generate a sizable signal at the sum frequency. A similar noise contribution can also be generated by the micromotion of the gate beam across the gate.

We can address this problem either by reducing the laser noise or by designing a gate that is impervious to laser fluctuations. The new picosecond sources now becoming available have significantly lower noise levels. As for redesigning the gate, we will begin by replacing the Schottky contact that forms the metal-semiconductor interface with an ohmic contact. This should greatly reduce the photovoltaic contribution from the gate. Since both the amplitude fluctuations and beam movement occur on the microsecond time scale, we can also introduce a feedback loop to cancel the photovoltaic signal. This would be accomplished by adjusting a voltage applied to the gate which is equal in amplitude but opposite in sign to its photovoltaic counterpart.

Another approach to improving sensitivity is to simply increase the gate pulse energy. To test this idea we increased the gate energy from 10 pJ/pulse to 70 pJ/pulse. This is sufficient to drive the gate below 10 Ω. The lower the gate resistance the higher the signal-to-noise. But there is a limit to how low the gate resistance can be made before the gate begins to saturate and the response time degrades. At 70 pJ/pulse, the response time increased by 40%. There are not many trades available to us that will allow a reduction in the gate resistance to $\leq 10\ \Omega$ and also attain a single-picosecond response. For picosecond response times we are restricted to a gate size no greater than $10 \times 10\ \mu m^2$.

On-going work with LT-InGaAs

For optical communications applications, the SOTA must operate between 1300-1600 nm. This means we will need to develop high speed InGaAs. During the latter part of this program we began growing LT-InGaAs structures and characterizing them for sensitivity, speed, resistivity, and optical absorption. The approach taken involves growing a InGaAs/InAlAs superlattice at low-temperature using MBE, followed with a 600° C anneal for 1 hour. For these structures, the LT-InGaAs serves as an absorbing layer while the LT-InAlAs serves as the carrier trapping layer. We discuss our initial results in this report. The superlattices were grown for us by the III-V Materials Group at Martin Marietta.

Lattice-matched LT-$In_{0.53}Ga_{0.47}As$ grown on InP has a resistivity of ~ 1 Ω-cm. In contrast, the resistivity for LT-GaAs is > 10^7 Ω-cm. To help us understand the effect indium has on resistivity we have grown a set of three lattice-matched samples and measured their sheet resistance. Figure 13 shows a curve of sheet resistance vs. indium concentration for the three samples. The three solid points represent sheet resistance values for lattice-matched LT-GaAs grown on GaAs, LT-$In_{0.35}Al_{0.65}As$ grown on a GaAs-based buffer layer graded from $In_{0.0}Al_{1.0}As$ to $In_{0.35}Al_{0.65}As$, and LT-$In_{0.53}Al_{0.47}As$ grown on InP. For reference we also show the sheet resistance for *polycrystalline* LT-$In_{0.35}Al_{0.65}As$. We see that the sheet resistance drops by 8 orders of magnitude from $3x10^{11}$ Ω/square to $5x10^3$ Ω/square as the indium concentration is increased from 0-53%. We have taken one of these samples, LT-$In_{0.35}Al_{0.65}As$ (sample M1331), and measured its transient optical reflectivity.

Figure 14 shows a family of four traces taken for as-grown GaAs as well as for increasing post anneal temperatures. For all time-resolved experiments described in this report we use a Ti:sapphire laser with pump-probe pulse durations of 0.1 ps and lasing at 800 nm. Despite the low sheet resistance, we see that LT-$In_{0.35}Al_{0.65}As$ has a carrier lifetime that is < 10 picoseconds. It is interesting to note that the annealing process has little effect on the carrier lifetime, with the as-grown and annealed lifetimes differing by at most a factor of two. The sheet resistance, on the other hand, was found to increase by 20-fold after annealing.

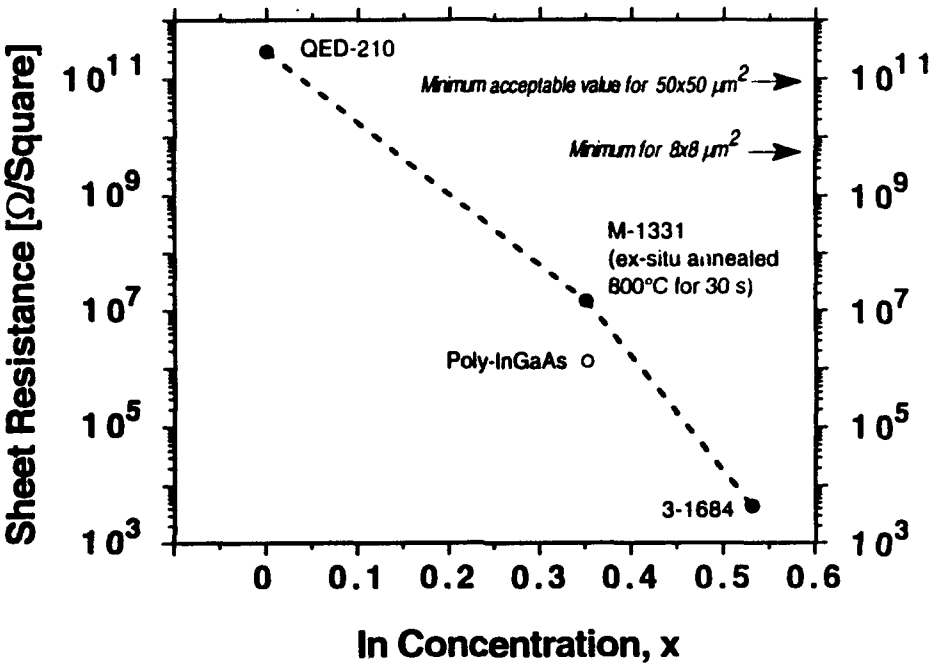

Fig. 13 Sheet resistance for post-annealed, lattice matched LT-GaAs, LT-$In_{0.35}Ga_{0.65}As$. LT-$In_{0.53}Ga_{0.47}As$. The sheet resistance for polycrystalline LT-$In_{0.35}Ga_{0.65}As$ is also shown. The minimum acceptable values for sheet resistance for detector areas of 50x50 μm^2 and 8x8 μm^2 are shown and correspond to a dark current of ~ 1nA.

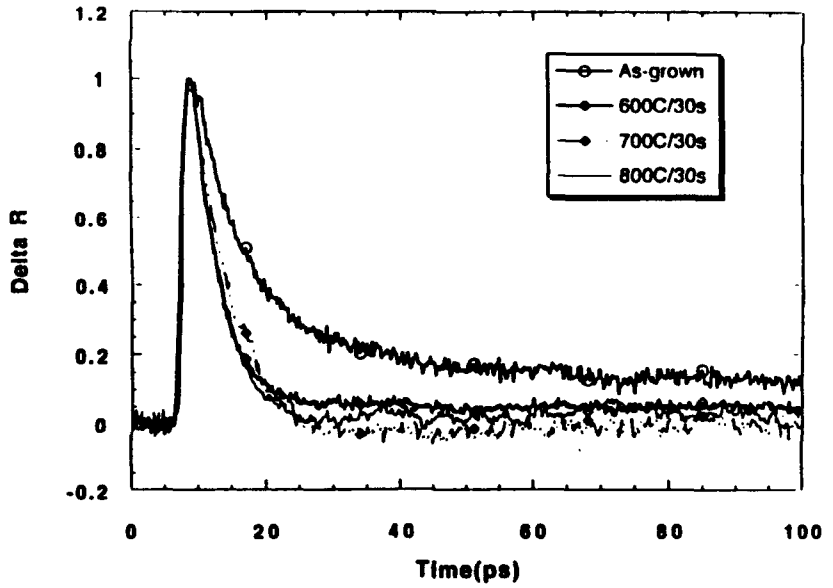

Fig. 14 Time-resolved all-optical transient reflectivity for $In_{0.35}Ga_{0.65}As$ pumped and probed with a 0.1-ps laser operating at 800 nm. The unannealed sample has a carrier lifetime of 14 ps (1/e), compared to 7 ps for the three post-annealed samples. Three of the samples were post annealed using a rapid thermal anneal (RTA) at 600°, 700°, and 800°C, respectively. The RTA time was 30 s.

A possible explanation for the low resistivity of InGaAs is offered in Fig. 15. Shown is a set of four simplified band diagrams for GaAs and InGaAs. The first diagram depicts the energy positions of the conduction and valence band edges, as well as the relative position of the Fermi level for unintentionally doped GaAs. We note that the Fermi level is at the midgap, 0.7 eV above the valence band.

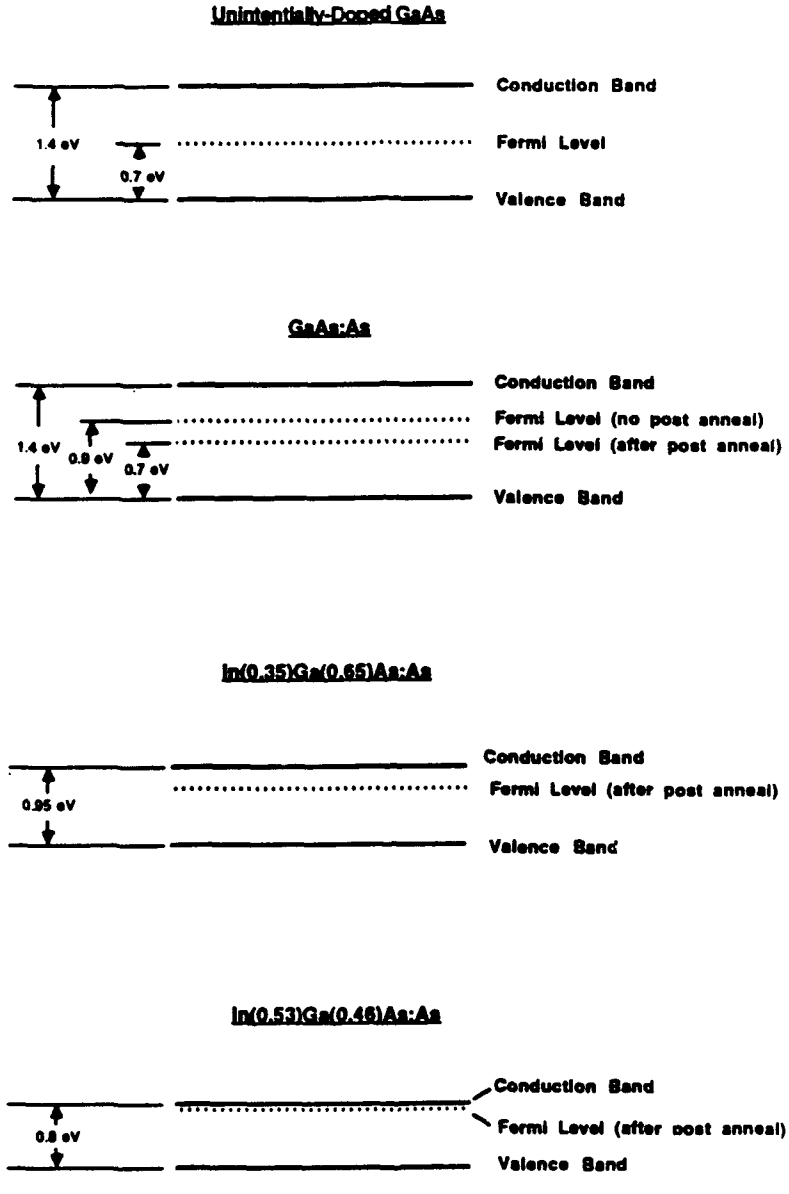

Fig. 15 Band diagrams for GaAs and InGaAs. After post annealing, the Fermi level for arsenic-rich GaAs returns to midgap. The presence of excess arsenic in InGaAs causes the Fermi level to move away from midgap and closer to the conduction band as the molar fraction of indium is increased.

Arsenic precipitates are deep-level trap that behave like dual deep donors and deep acceptors to render the material semi-insulating. In the second diagram we show LT-GaAs with upwards of 10^{19} cm^{-3} arsenic antisite defects being pinned 0.9 eV above the valence band. After annealing the arsenic antisites aggregate into Schottky precipitates with a pinned barrier height of 0.7 eV. The difference in sheet resistance for these two states is significant, 10^3 Ω/square vs. 10^{11} Ω/square for the unanneal and post annealed, respectively. The third diagram shows the band structure for LT-$In_{0.35}Ga_{0.65}As$. The Fermi level is no longer at midgap but pinned closer to the conduction band. The semiconductor in this case is n-type which yields considerably higher sheet resistance. The last diagram shows the band structure for LT-$In_{0.53}Ga_{0.47}As$. The Fermi level is pinned just below the conduction band, resulting in an extremely high concentration of thermally-ionized carriers.

We now describe one approach we are taking to attempt to increase the resistivity for LT-InGaAs. This approach separates the absorption and trapping processes by utilizing a superlattice structure formed of LT-InGaAs and LT-InAlAs.

LT-$In_{0.53}Ga_{0.47}As$ / LT-$In_{0.52}Al_{0.48}As$ Superlattice This photoconductor utilizes high resistivity, fast carrier lifetime LT-InAlAs combined in a superlattice with LT-InGaAs to achieve fast response time with low dark current. $In_{0.52}Al_{0.48}As$ is lattice matched to InP and $In_{0.53}Ga_{0.47}As$. It has a bandgap close to that of GaAs, making it of little use for long-wavelength detectors on its own. By growing alternate layers of absorbing InGaAs and InAlAs we will be able to both absorb the long-wavelength optical signal and trap the carriers. We have grown LT-$In_{0.53}Ga_{0.47}As$ / LT-$In_{0.52}Al_{0.48}As$ superlattices on InP with 200-Å layer thicknesses to demonstrate the concept. We chose the 200 Å thickness to be close to the spacing of the precipitates normally found in LT-GaAs.

Figure 16 shows the absorption curve for the superlattice structure, along with its layer profile. The structure was grown on semi-insulating InP starting with a 1000-Å layer of $In_{0.52}Al_{0.48}As$ grown at normal stoichiometric temperature (520° C) and followed by a second 1000-Å layer of $In_{0.52}Al_{0.48}As$ grown as the temperature dropped from 520° C to 245° C. The superlattice was then grown with alternating layers of 200-Å thickness $In_{0.53}Ga_{0.47}As$ and $In_{0.52}Al_{0.48}As$, and capped with a 200-Å layer of $In_{0.53}Ga_{0.47}As$. The sample was then post annealed at 470° C for 10 minutes in an arsenic overpressure. The action of post annealing causes excess arsenic in the InGaAs layer to be gettered into the adjacent InAlAs layers, where is

aggregates into precipitates of similar size and spacing as found in bulk grown LT-InAlAs. The 200 Å thickness assures that the InGaAs will be fully depleted. Going larger than 200 Å for the InGaAs thickness might reduce the effect of the Schottky precipitates. Going thinner of course reduces the effective absorption. We also selected 200 Å for the InAlAs layer, which simplified the growth procedure and assured a sufficiently thick region to trap carriers.

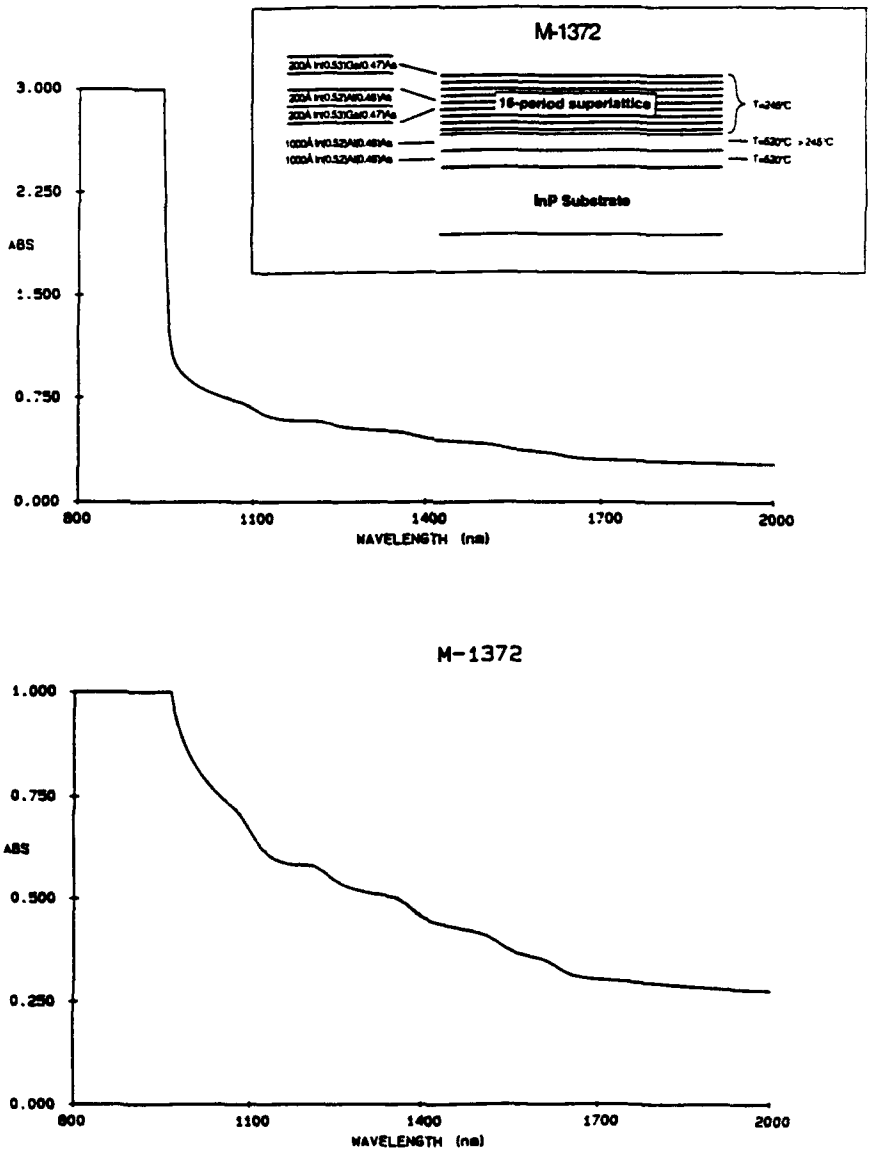

Fig. 16 Spectraphotometer scan of LT-$In_{0.53}Ga_{0.47}As$/LT-$In_{0.52}Al_{0.48}As$ superlattice (shown in insert). Absorption (ABS) is plotted in OD. The relation between the measured absorption and the absorption coefficient, α is: $\alpha[cm^{-1}] = -(1/T[cm])\ \ln\ (10^{-ABS[OD]})$, where T is the epilayer's thickness. The ripples on the curve are due to the periodicity of the superlattice.

The ripples that appear on the absorption curve of Fig. 16 correspond to the periodicity for multiple quantum wells of 200 Å spacing. We expect to see an absorption edge approximately midway between the absorption edge for $In_{0.52}Al_{0.48}As$ (825 nm) and $In_{0.53}Ga_{0.47}As$ (1550 nm), or ~1188 nm. It is difficult to discern from the surrounding features whether the 1550-nm edge exist. The sheet resistance for bulk LT-$In_{0.52}Al_{0.48}As$ is 10^9 Ω/square. The sheet resistance for the low-temperature grown superlattice is 10^6 Ω/square, 500-fold improvement over bulk LT-$In_{0.53}Ga_{0.47}As$.

The dynamics for charge transport go as follows. Light is absorbed in the InGaAs layers creating electrons and holes. In the presence of a moderate electric field (10^3 V/cm) applied in the plane of the layers the photogenerated carriers are accelerated to sufficiently high energy to overcome the barrier potential and transfer into the wide bandgap InAlAs layers. Given the mobility for InGaAs and the 200-Å layer thickness, real space transfer should take 2-5 picoseconds. Once in the arsenic-rich LT-InAlAs layers the carriers are trapped within a few picoseconds. The presence of the electric field is important to accelerate the carriers and affect the thermionic emission process. If the field is perpendicular to the layers the carriers will accumulate at the interface and will be slow to tunnel through the interface. If sufficiently large light levels are absorbed in both the InGaAs and InAlAs, the 0.25-eV barrier will taper off via band bending to allow carriers to move more freely through the interface, even with no field applied.

This latter case was the set of conditions used to initially study charge transport in our samples. Figure 17 shows the transient reflectivity for the superlattice with a laser operating at 800 nm was used to produce electron-hole pairs. In this experiment carriers are generated both in the LT-$In_{0.53}Ga_{0.47}As$ and LT-$In_{0.52}Al_{0.48}As$. The reflectivity shows that the material is indeed as fast as bulk LT-$In_{0.52}Al_{0.48}As$. Time-resolved photoconductive measurements, with the light selectively absorbed by the InGaAs layers, are now needed to determine the true carrier lifetime for this material. These initial results are nevertheless encouraging.

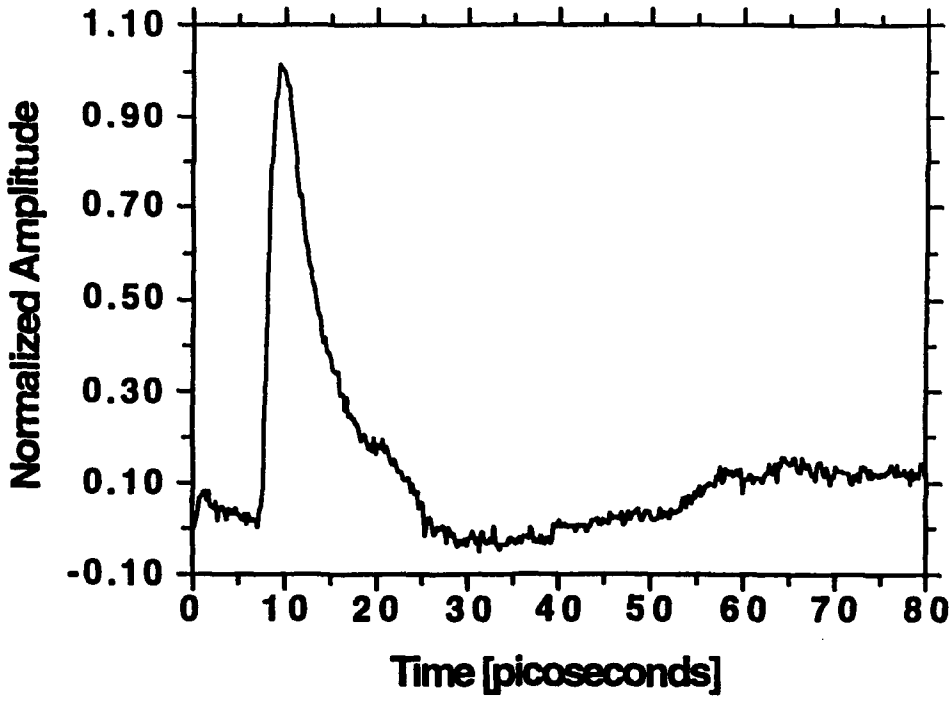

Fig. 17 Transient reflectivity of the LT-$In_{0.53}Ga_{0.47}As$/LT-$In_{0.52}Al_{0.48}As$ superlattice. The measurement was made with both the pump and probe light being above the bandgap for the LT-$In_{0.52}Al_{0.48}As$. Hence, carriers were photogenerated in both layers. Despite the suboptimal laser wavelengths, we see that the superlattice has a effective carrier lifetime of 8 picoseconds (1/e). The carrier lifetime of unintentionally-doped $In_{0.53}Ga_{0.47}As$ is several hundred picoseconds.

5. CONCLUSIONS

We have demonstrated the use of a novel all-solid-state optical detector integrated with a picosecond analyzer that form the world's fastest, most compact, ultrasensitive, picosecond optical waveform analyzer. The output from this device is a quasi-DC current that can be measured using conventional electronics. The speed, sensitivity, and dynamic range of the SOTA, coupled with its ability to be mass produced using conventional microfabrication, offers us a unique opportunity to develop a new and greatly advanced generation of ultrafast optoelectronic technology.

The application of the SOTA as an high-speed AND-gate is one example. At this time, the picosecond SOTA is limited to wavelengths at or below 900 nm. In the near future, as novel nonstoichiometric InGaAs-based materials improve, the unique performance of the SOTA will play an important role in ultrafast communications.

6. REFERENCES

1. Y. Chen, S. Williamson, T. Brock, F. W. Smith, A. R. Calawa, Appl. Phys. Lett. **59**, 1984, 1991.
2. S. M. Sze, *Physics of Semiconductor Devices*,, 2nd. ed., (Wiley, New York, 1981), p. 746.
3. J. F. Whitaker, J. A. Valdmanis, M. Y. Frankel, S. Gupta, J. M. Chwalek, and G. A. Mourou, Microelectron. Eng. **12**, 369 (1990).
4. Y.G. Wey, D.L. Crawford, K. Giboney, J.E Bowers, M.J. Rodwell, Appl. Phys. Lett. 58, 19, 2156, 1991.
5. D. H. Auston, *Picosecond Optoelectronic Devices*, ed. C. H. Lee, (Academic Press, Inc. New York, 1984), p. 73.
6. D. R. Grischkowsky, M. B. Ketchen, C-C. Chi, I. N. Duling III, N. J. Halas, J-M. Halbout, IEEE J. Quantum Electron. **24**, 221 (1988).
7. F.W Smith, Ph.D thesis, Massachusetts Institute of Technology, Cambridge, MA, 1990.
8. S. Gupta, Ph.D thesis, Univ. of Michigan, Ann Arbor, MI, 1992.

*U.S. GOVERNMENT PRINTING OFFICE: 1994-510-117-50042

MISSION

OF

ROME LABORATORY

Mission. The mission of Rome Laboratory is to advance the science and technologies of command, control, communications and intelligence and to transition them into systems to meet customer needs. To achieve this, Rome Lab:

a. Conducts vigorous research, development and test programs in all applicable technologies;

b. Transitions technology to current and future systems to improve operational capability, readiness, and supportability;

c. Provides a full range of technical support to Air Force Materiel Command product centers and other Air Force organizations;

d. Promotes transfer of technology to the private sector;

e. Maintains leading edge technological expertise in the areas of surveillance, communications, command and control, intelligence, reliability science, electro-magnetic technology, photonics, signal processing, and computational science.

The thrust areas of technical competence include: Surveillance, Communications, Command and Control, Intelligence, Signal Processing, Computer Science and Technology, Electromagnetic Technology, Photonics and Reliability Sciences.